Structural Identification of Mir using Inverse System Dynamics and Mir/Shuttle Docking Data

Daniel C. Kammer
Associate Professor

and

Adam D. Steltzner
Research Assistant

Department of Engineering Physics
University of Wisconsin
Madison, WI 53706

Abstract

The goal of this work was to determine if it is feasible to use Mir/Shuttle docking data to perform Mir damage detection. A time-domain technique called a Remote Sensing System was proposed as an approach. The method uses inverse structural dynamics to identify physical characteristics of a structure which can subsequently be used for damage detection. The RSS method was demonstrated for a numerical simulation of Mir/Shuttle docking assuming that sensors were collocated with Mir docking location. Several fixed interface Mir modes were identified from the computed RSS pulse responses using the Eigen System Realization Algorithm and then correlated with ta finite element representation. The method was then applied to the combined set of docking data from Mir/Shuttle missions STS-81, STS-89, and STS-91. Two modes were identified that correlated very well with FEM fixed interface modes. Finally, projections of the Mir and FEM RSS pulse responses onto the individual docking data sets were compared for changes in the structure. Overall, the results produced by this work appear to indicate that Mir was in an undamaged state, at least with respect to docking excitation, at the time of STS-91. The significance of the contribution of the RSS approach is that it is not affected by the nonstationarity and nonlinearity associated with the Mir/Shuttle docking interface, and docking forces at the interface do not have to be measured.

I. Introduction

During the course of the Mir-Shuttle program, the structural integrity of Russia's Mir Space Station, pictured in Fig. 1, was a major concern due to Mir's longevity. The potential problem was exacerbated when a Progress supply ship collided with Mir during the summer of 1997. Mir therefore represents a rare opportunity to evaluate methods for detecting damage on an actual structure in orbit. Currently, modal identification is a very popular approach to damage detection. Pre- and post-damage vibration experiments are performed and damage is detected by observing changes in frequencies and shapes of excited modes. Reference [1] presents a comprehensive review of modal based damage detection techniques. In the case of Mir, there are several possible sources of excitation, such as Mir and Shuttle thruster firing, intentional crew motion, ambient noise, and docking events. In general, it was observed that Shuttle docking produced the largest structural responses in Mir [2].

Modal identification of Mir using docking data represents a formidable challenge for several reasons. First, modal identification techniques in general work best when there is a sufficient amount of data available for averaging. In the case of Mir, the short time duration of the docking events coupled with the availability of a relatively small number of data sets precluded averaging. In addition, if the measured Mir response to docking is considered as free-decay of a coupled Mir-Shuttle system, the combined structure is nonlinear due to the docking element, and the system is time-varying due to non-instantaneous capture. Free-decay identification techniques, such as the Eigensystem Realization Algorithm (ERA) [3], cannot easily be applied to this problem. In order to avoid the effects of nonlinearities and the time-varying configuration, Mir docking response can alternatively be considered as forced response due to the shuttle acting as a large shaker. Typically, during a modal test, both the force inputs and the response of the system are measured. Frequency response and pulse response functions are generated and many methods are then applicable for modal identification. In the case of Mir, the docking forces that excite the space station are not measured, limiting the number of techniques available for modal identification. Two output-only approaches that are applicable include the Natural Excitation Technique (NExT) [4] and subspace identification algorithms [5]. However, these and related methods assume that the input to the system is white noise. The docking forces applied to Mir clearly do not fit this criterion.

The objective of the work presented here is to investigate the use of inverse system identification techniques on Mir/Shuttle docking data to identify Mir vibrational characteristics for ultimate application to damage detection. This new approach, initially presented by Kammer in Ref. [6], does not attempt to identify the usual mode shapes and frequencies of a structure. Instead it identifies the vibrational characteristics of an inverse representation. A system's inverse representation differs from the usual forward representation in that the roles of the input and output are reversed. The associated inverse vibrational characteristics consist of frequencies and mode shapes for the inverse system. In special cases, they represent quantities as closely related to the forward system as constrained modal parameters. In this situation, inverse frequencies and mode shapes can be easily related to structural parameters and characteristics. Changes in the inverse

modal parameters can then be related to corresponding changes in the structure. The main advantages of using the inverse system identification approach are that the force inputs to the structure do not have to be known and there are no requirements for the input forces to be random or stationary.

The paper first gives a brief presentation of the inverse system identification theory. Details can be found in Ref. [6]. New results involving cases with varying relations between numbers of reference sensors, inputs, and experimental data sets are discussed. The inverse identification approach is then applied to a detailed numerically simulated docking example involving a finite element representation (FEM) of Mir. Finally, the method is applied to actual measured docking data from STS-81, STS-89, and STS-91. Docking response was recorded using the Russian Mir Structural Dynamic Measurement System (SDMS) which included 25 piezoelectric accelerometers. Results are then compared with the FEM and the simulated docking analyses.

II. Theory

The inverse system identification approach is based upon a technique previously developed by Kammer [7] for measuring the response of an operating structure at discrete locations and predicting the response at other desired locations on the structure that do not have sensors during operation. It was shown that an input-output representation called a Remote Sensing System (RSS) can be derived directly from vibration test data where the input is the measured response at the sensor locations and the output is the desired remote location response. It is assumed that in discrete time, the structure can be represented by the difference equation

$$x(k+1) = Ax(k) + Bu(k) \tag{1}$$

in which x represents an n dimensional state vector, A is the nxn system matrix, B is the nxn_a input influence matrix, and u is the n_a dimensional force vector. The corresponding system output equation is given by

$$y_s(k) = C_s x(k) + D_s u(k) \tag{2}$$

where y_s is an n_s dimensional sensor output vector, C_s is an n_sxn output influence matrix, and D_s is an n_sxn_a direct transmission matrix. Accelerometers are used as sensors such that the direct transmission matrix is nonzero, however, other types of sensors can be used by appropriately modifying the derivations using lagged systems. It is also assumed that the structure being considered is free-free.

An analytical representation of the RSS can be derived by solving Eq. (2) for the force input at time step k

$$u(k) = -D_s^+ C_s x(k) + D_s^+ y_s(k) \tag{3}$$

in which D_s^+ represents the generalized inverse $D_s^+ = \left(D_s^T D_s\right)^{-1} D_s^T$. Note that the number of sensors n_s must be greater than or equal to the number of inputs n_a. Equation (4) is then substituted into the state equation (1) producing

$$x(k+1) = \hat{A}x(k) + \hat{B}y_s(k) \tag{4}$$

where the new plant and input influence matrices are given by

$$\hat{A} = A - BD_s^+ C_s \qquad \hat{B} = BD_s^+ \tag{5}$$

Equations (3) and (4) represent an inverse system in which the roles of input and output have been reversed with respect to the forward system in Eqs. (1) and (2). The forward system output equation for the response at the desired n_d remote locations is analogous to Eq. (2)

$$y_d(k) = C_d x(k) + D_d u(k) \tag{6}$$

Substituting for the input force from Eq. (3) produces

$$y_d(k) = \hat{C}x(k) + \hat{D}y_s(k) \tag{7}$$

with

$$\hat{C} = C_d - D_d D_s^+ C_s \qquad \hat{D} = D_d D_s^+ \tag{8}$$

Equations (4) and (6) represent the RSS in which measured response is the input and desired response is the output. The input force acting on the structure has been completely eliminated from the system equations. It is important to note that the state equations for both the inverse system and the RSS are identical.

Alternatively, the RSS can be represented by the convolution

$$y_d(k) = \sum_{i=0}^{k} P_i y_s(k-i) \tag{9}$$

in which the n_d x n_s weighting matrices P_i are the RSS Markov parameters. They represent the free-decay response of the RSS and thus a modal identification technique such as ERA can be used to identify the corresponding RSS mode shapes and frequencies. Equations (4), (5), (7), and (8) show that the RSS and its modal parameters depend directly upon the physical parameters of the actual structure and can be used to detect structural damage.

A. Inverse System Modal Parameters

In order to be a useful tool, it is important to determine the physical significance of the RSS or inverse system eigenvalues and corresponding mode shapes when possible. The interpretation is dependent upon the relationship between the numbers and locations of forward system inputs and outputs. For the special case where there are as many sensors as force inputs, $n_s = n_a$, it can be shown [6] that the inverse system eigenvalues are equivalent to the forward system transmission zeros. Transmission zeros are defined to be the complex values ψ at which it is possible to apply a nonzero input, $u = \mu e^{\psi t}$, and get an identically zero output at the sensor locations for suitable initial conditions $x(0)$. Williams [8] can be consulted for more details on transmission zeros and structures.

Corresponding to the particular case of equal numbers of inputs and outputs, two possible subcases are considered. In the first subcase, the inputs and outputs are totally noncollocated, meaning that there are no sensors at any of the input locations. In this situation, the forward system is in general nonminimum phase [9]. This means that some of the transmission zeros of the discrete forward system are outside the unit circle, or for the continuous representation, in the right half plane, which implies that the inverse system has unstable poles. The corresponding RSS Markov parameters in Eq. (9) grow without bound. The remaining stable inverse system eigenvalues occur in complex conjugate pairs. It was shown in Ref. [6] that the proposed RSS identification technique estimates the minimum phase portion of the RSS pulse response corresponding to the stable transmission zeros and related shapes that are inside the unit circle for the discrete system.

The second subcase of special interest with respect to identification is one in which sensors and outputs are collocated. In this situation, every force input location and direction has a corresponding sensor. In addition, it is assumed that the sensors are just sufficient in number and location to remove all rigid body modes from the structure if constrained. In this case, Ref. [6] illustrated that a Craig-Bampton representation [10] of the structure computed relative to the sensor locations is equivalent to an inverse structural system in which the acceleration at the sensor locations is the input to a fixed mode state equation and the output is the force applied at the sensor locations. Therefore, in the rigid body sufficient collocated case, the RSS eigenvalues and mode shapes correspond to the frequencies and mode shapes of the structure with the sensor degrees of freedom fixed. This is a strong result in that many techniques exist for relating physical changes in structures to corresponding changes in the structure's modal parameters.

B. Identification of RSS Markov Parameters

Before modal parameters can be identified, the RSS pulse response must be estimated using experimental data. The available data is split into the two previously discussed sets, the sensor locations numbering n_s and the desired locations numbering n_d. Note that the n_s sensor locations can be considered as references analogous to input locations in a usual vibration test. If there are n_e experiments, the RSS convolution equation (9) can be expanded into the matrix equation

$$PY_s = Y_d \tag{10}$$

where

$$P = \begin{bmatrix} P_0 & P_1 & \cdots & P_{N_R-1} \end{bmatrix} \qquad Y_d = \begin{bmatrix} y_{d0} & y_{d1} & \cdots & y_{dn_t-1} \end{bmatrix}$$

$$Y_s = \begin{bmatrix} y_{s0} & y_{s1} & \cdots & \cdots & y_{sn_t-1} \\ 0 & y_{s0} & \cdots & \cdots & y_{sn_t-2} \\ 0 & 0 & \vdots & \cdots & \vdots \\ \vdots & \vdots & \vdots & \cdots & \vdots \\ 0 & \cdots & y_{s0} & \cdots & y_{sn_t-N_R} \end{bmatrix}$$

and y_{si} is an $n_s \times n_e$ matrix in which the *j*th column represents the measured sensor response at time step *i* for experiment *j*, y_{di} is the corresponding response at the desired locations, and n_t is the number of experimental data points. In an application, the data matrices in Y_s and Y_d are truncated to N_C block columns. Two cases important to RSS modal identification are considered.

1. Equal Numbers of Sensors and Experiments

In this case, the data blocks y_{si} are assumed to be square and full rank. The corresponding data matrix Y_s theoretically should then be full row rank. If equal numbers of block rows and block columns are used, i.e. $N_R = N_C$, Y_s is square and the first N_R RSS Markov parameters can be determined uniquely by inverting Y_s in Eq. (10). In practice, the data matrix Y_s becomes very large and ill-conditioned. The usual matrix inverse is replaced by a Moore-Penrose pseudo-inverse based upon singular value decomposition [11]. In general, for computational stability, the problem is made to be overconstrained by adding block columns such that $N_C > N_R$. The solution for the RSS pulse response is then given by

$$P = Y_d Y_s^T \left(Y_s Y_s^T \right)^+ \tag{11}$$

where the superscript + denotes the pseudo-inverse. The normal form of the least-squares solution is used at the risk of inaccuracy in order to minimize the memory requirements for the pseudo-inversion of the data matrix. More efficient and accurate solution techniques will be investigated in future research. Once the RSS pulse response is identified, ERA can be used to extract the corresponding modal parameters.

2. More Sensors than Experiments

In Kammer's original development and application [7], identification of the RSS model was based upon the forward system pulse response measured during a vibration test. In this case, the number of experiments is equal to the number of inputs, $n_e = n_a$. The goal was to compress the system information contained in the RSS Markov parameters in the pulse response sequence into a

much smaller number of equivalent terms or weighting matrices W_i. This was accomplished by using several more sensors (references) than experiments and many more block columns than block rows. It is believed that this compression is analogous to that produced by the observer formulation introduced in Refs. [12, 13]. The only requirement is that the product $N_R \cdot n_s$ must be greater than the number of observable-controllable modes responding in the data. Due to the relatively small number of block rows used, the computation of the system equivalent RSS weighting matrices using Eq. (11) was observed to be very robust to data errors and noise. Unfortunately, the estimated weighting sequence representation cannot be directly used as free-decay data in ERA to estimate the RSS modal parameters.

The Mir damage detection problem using docking data represents a case where the number of sensors is greater than the number of available experiments. During this project, there was only one set of docking data available from before the Mir/Progress collision, STS-81, and two from after the collision, STS-89 and STS-91. Damage detection requires the comparison of RSS results computed using the single data set from STS-81 with results produced from the individual post-damage data sets. Ideally, there are three forces and three moments acting on Mir through the docking mechanism. In order to avoid compression when estimating the RSS pulse response in this case, the number of block rows and columns must be the same. This situation produces a data matrix Y_{si}, corresponding to the *i*th docking data set, that has more rows than columns and the corresponding matrix Eq. (10) is underdetermined. There are now an infinite number of solutions. A solution with minimum norm can be obtained using the formulation

$$\hat{P}_i = Y_{di}\left(Y_{si}^T Y_{si}\right)^+ Y_{si}^T \tag{12}$$

If P is the true RSS pulse response, $\hat{P}_i$ represents the orthogonal projection [14] of P onto the column space of data matrix Y_{si} given by

$$\hat{P}_i = PY_{si}\left(Y_{si}^T Y_{si}\right)^+ Y_{si}^T = PH_i \tag{13}$$

As in the case of the compressed weighting sequence, the orthogonal projection of the pulse response cannot be directly used in ERA to estimate the RSS modal parameters. In addition, estimates of orthogonal projections produced by two different experiments will in general be different and thus cannot be directly compared for the purpose of detecting structural changes.

Alternatively, it could be assumed that enough docking data sets have been accumulated during the early life of the structure such that the RSS pulse response of the undamaged structure, P, can be computed using Eq. (11). A data set from a subsequent docking event can then be used to detect any damage that may have occurred since the docking event that produced the last data set used in the identification of the RSS pulse response. Considering only the new docking data set, Eq. (12) can be used to compute $\hat{P}_i$ corresponding to the projection of the RSS pulse response onto the vector space spanned by the data set. Using the orthogonal projector H_i from Eq. (13),

the undamaged RSS pulse response P can be projected onto the same vector space to produce P_i. If P was originally computed using equal numbers of block rows and block columns in its data matrix Y_s and if the structure remains undamaged, then $\hat{P}_i = P_i$. Lack of agreement indicates damage. When the conditions mentioned are satisfied, the equality holds in general because the n_e individual data matrices Y_{si} used to produce Y_s in Eqs. (10) and (11) have independent column spaces. This implies that P_i is due only to the data from the ith docking event and should thus agree with $\hat{P}_i$. For FEM simulated docking data, the equality holds even for the overconstrained case where the number of block columns is much greater than the number of block rows. In general, overconstraint is required for computational stability. Unfortunately, real data is not consistent, therefore the equality $\hat{P}_i = P_i$ does not hold in general in the overconstrained case. Future work will address this shortcoming of the RSS approach as applied to docking data.

Alternatively, there is an a posteriori approach that can be used to compare individual docking data sets and search for damage between docking events. The method is not ideal because enough post-damage data sets must be accumulated to identify a new RSS pulse response using Eq. (11). The procedure will be demonstrated for real docking data in Section IV.

III. Numerical Example

The use of the RSS identification approach is first demonstrated for a case where there is sufficient data to perform pulse response identification. A numerical example is presented in which docking is simulated for Mir using the Russian built FEM supplied by NASA. The FEM shown in Fig. 2 is an equivalent beam representation containing 2,646 dof and 211 free-free modes with frequencies below 5.0 Hz. Three independent docking experiments were simulated, each with three input forces in the *x*, *y*, and *z* directions at the docking node 118009. Moments applied at the docking node were ignored for computational efficiency. The first set of docking forces was simulated by scaling the translational response of the accelerometer at node 105011 on the Krystall module measured during STS-81. The *x* and *y* responses were multiplied by $2g$, while the *z* response was multiplied by $20g$. Figure 3 illustrates the corresponding docking forces for experiment 1. The translational forces analytically reconstructed by NASA for STS-81 were used in experiment 2 and the translational response measured at node 105011 during STS-89 and scaled by the same factors as in experiment one were used as docking forces in experiment 3. Two percent critical damping was assumed for all 211 modes in the simulations.

During the simulated docking experiments, three accelerometers were assumed to be collocated with the force input locations. Therefore, the numbers of sensors, inputs, and experiments are all equal to three in this example. The inverse system eigenvalues and mode shapes will correspond to Mir structural modes with the three translational degrees of freedom at the sensor locations fixed. Desired response locations were chosen to coincide with the 25 accelerometer locations on Mir. Table 1 lists the locations and corresponding FEM node numbers in the order in which data channels were measured during STS-81. Figure 2 shows the corresponding FEM node locations. During the docking experiments, it was assumed that the

acceleration was also measured at the desired location set just as would be the case during an actual docking event.

Each experiment was simulated in MATLAB for 1,150 time steps of 0.02 seconds each. In order to simulate errors and noise in the measured data, normally distributed zero mean random noise, equivalent to 5.0% of the root-mean-square (rms) response, was added to each of the 3 sensor and 25 desired response channels from each experiment. The RSS pulse response was computed by generating a sensor data matrix with 650 block rows and 1,100 block columns producing a 1,950 by 3,300 matrix. Note that the added noise actually helps stabilize the computation of the pulse response in this example. A typical RSS pulse response from sensor location 118009z to desired response location 102015z is pictured in Fig. 4 after it has been low pass filtered to 5.0 Hz.

The Eigensystem Realization Algorithm (ERA) was then applied to the estimated noisy RSS pulse response data. Eighty singular values were retained and 38 mode shapes and frequencies were computed using a block Hankel matrix with 30 block rows and 500 block columns. Three indicators of goodness were used to distinguish true modes from noise. The first indicator, *Modal Amplitude Coherence* (MAmpC) [11], gives a measure of how well a computed mode shape and frequency reproduce the measured system response. A value of 1.0 indicates perfect reproduction. The second indicator, *Modal Phase Collinearity* (MPC) [15], gives a measure of the degree of monophase or normal behavior of an extracted mode shape. Its value ranges from 0.0 to 100.0 percent for a perfect normal mode. Finally, the *Mode Singular Value* (MSV) [11] gives a measure of the contribution of each mode to the identified pulse response time history. The measure is normalized such that the strongest responding mode has an MSV value of 1.0.

Based upon the values of the estimated frequencies, damping, and the three measures of goodness, five modes were selected from the estimated mode set. Table 2 presents the identification results for the selected modes, including fraction of critical damping, frequency, and the three indicator values. Note that the damping is not accurately estimated, probably due to the small amount of data used in the identification. The linear independence of the identified modes was examined using the Modal Assurance Criterion (self-MAC) [16] which is given by

$$MAC_{jk} = \frac{\left|\phi_j^T \phi_k\right|}{\left(\phi_j^T \phi_j\right)\left(\phi_k^T \phi_k\right)} \tag{15}$$

for the *j*th and *k*th modes. The diagonal terms of the self-MAC matrix are normalized to 100.0 and the off-diagonal values essentially represent the cosine of the angle between each of the identified modes. Off-diagonal terms less than or equal to 10.0 indicate that the identified mode shapes are independent. Table 3. lists the self-MAC matrix for the identified mode shapes. All off-diagonal terms are less than 10.0, indicating that the mode shapes are independent. The five modes identified from the simulated docking data were then compared with the 209 mode shapes predicted by the Mir FEM below 5.0 Hz. with the three sensor degrees of freedom at the docking point fixed. Estimated docking modes and fixed sensor FEM modes were matched based upon cross-

MAC shape comparison and frequency. Table 4 lists docking/FEM mode pairs with cross-MAC values and the corresponding frequency errors. Because of the relatively small number of accelerometers used in the modal identification, the estimated docking modes are highly coupled with several of the FEM mode shapes.

The simulated test/FEM mode pairing listed in Table 4 was further investigated by computing a reduced mass matrix, called a Test-Analysis Model (TAM), which possessed only the 25 desired sensor location degrees of freedom. The very small number of degrees of freedom forced the use of an advanced technique called Modal reduction [17] to produce the TAM. A Modal TAM was generated that exactly predicted the five FEM modes that were paired with the simulated test modes. Cross-orthogonality was then computed between the FEM and test modes using the relation

$$CGM = \phi_{FEM}^{T} M_{TAM} \phi_{Test} \tag{16}$$

where ϕ_{FEM}, ϕ_{Test}, and M_{TAM} are the FEM modes, test modes, and TAM mass matrix, respectively. Table 4 lists the cross-generalized mass values scaled to a perfect value of 100.0 for each of the simulated test/FEM mode pairs. All values are well above 80.0 indicating good mass weighted shape agreement. Based upon cross-MAC values that are approximately 90.0 and larger, frequency errors that are less than 4.0%, and CGM values greater than 80.0, it is believed that the RSS/ERA approach accurately identifies five sensor fixed FEM modes using docking data with 5.0% noise. Note that Table 2 indicates that simulated test mode 1, which correlates with FEM mode 80, is the most strongly excited of the test modes identified (MSV = 1.00). This agrees with the fact that FEM mode 80 possesses the greatest amount (27%) of Effective Mass [18] in the z direction for the constrained structure. It is expected that the largest docking forces act along the line of docking or the z axis, therefore mode 80 should be strongly excited. Figure 5 illustrates FEM mode 80 which can be seen to have a substantial amount of z motion as expected.

An objective of this numerical experiment was to determine if the proposed RSS identification technique can be used in conjunction with the relatively small amount of data provided by Mir/Shuttle docking events to detect structural changes or damage in the Mir primary node, specifically at the Krystall-to-base module interface. One of the major difficulties associated with using docking data for modal identification is that the excitation due to the docking forces is neither persistent nor broadband, as evidenced by the identification of only five modes from the numerical experiment. Each of the identified FEM modes was examined for its strain energy content within the primary node interfaces. Of the five, mode 80 contains over 80.0% of its modal strain energy within the primary node interfaces and mode 91 contains 16.8% within the interfaces. The remaining three modes contain insignificant amounts of strain energy in this area.

Unfortunately, essentially none of the strain energy in modes 80 and 91 corresponds to the spring elements associated with the Krystall-to-base module interface. Within mode 80, the energy is evenly divided between the *x* direction torsional spring element 104400 at the Kvant-2-to-base module interface and the *x* direction torsional spring element 107400 at the Spektr-to-base module

interface. Within mode 91, 11.2% of the strain energy is contained in the *z* direction torsional spring element 104600 at the Kvant-2-to-base module interface and 5.5% is contained in the *z* direction torsional spring element 107600 at the Spektr-to-base module interface. Inspection of the remaining sensor fixed FEM modes shows that a significant amount of strain energy does not appear in the Krystall-to-base module interface until mode 182 at 4.021 Hz., and mode 195 at 4.495 Hz. Neither of these modes was strongly excited and thus not identified from the simulated docking data. Based upon this example, it appears that damage in the Krystall-to-base module interface cannot be identified from docking data.

While it isn't possible to detect damage in the Krystall-to-base module interface, it does appear feasible to identify structural changes in either the Kvant-2-to-base module or Spektr-to-base module interfaces by monitoring frequency changes in test modes corresponding to FEM mode 80. The docking simulation and subsequent identification produced an accuracy of 1.57% for the frequency of mode 80. It has been common practice in modal testing and FEM model updating to regard a test/FEM frequency difference of less than 5.0% to be very good test-analysis correlation. It is obvious that the threshold for the existence of damage or correlation depends strongly on the application, but it would seem that at least a 5.0 to 10.0% change in frequency would then have to occur to be able to differentiate between a good frequency identification and actual damage. Design sensitivity analysis using the undamaged FEM indicates that to get the lower bound 5.0% change in frequency for mode 80 would require approximately a 25% decrease in the interface stiffness. This is probably an unacceptably high threshold for the detection of damage in a critical component. It is important to note that the described sensitivity problem for this particular application is not due to the RSS identification technique presented in this paper. Any damage detection technique using docking data and subsequent shifts in identified frequencies would have the same problem.

IV. Application of RSS to Mir/Shuttle Docking Data

The RSS identification technique will now be applied to actual docking data from the STS-81, STS-89, and STS-91 missions. Docking response was recorded using the Russian Mir Structural Dynamic Measurement System (SDMS) which included 25 piezoelectric accelerometers. This measurement system has a fixed frequency range of 0.1 to 5.0 Hz and a fixed dynamic range of 1.5 to 30.0 milli-g. Analog acceleration is telemetered directly to the ground and then processed with a sampling rate of 50.0 Hz. Data loss during telemetry can be as high as 15.0% [2]. Further details can be found in Ref. [2]. All docking data was low-pass filtered to 5.0 Hz prior to being received from NASA. Unfortunately, only 19 accelerometer locations are common to all three docking events. The triax on the Spektr module was lost to STS-89 and STS-91 due to the collision with the Progress spacecraft and data from the triax on Priroda was not included in the STS-91 data set for unknown reasons. In the subsequent analyses, it is assumed that the docking forces dominate the response of Mir while the effects of the moments are secondary. This is consistent with results presented in Ref. [19]. Three RSS reference sensors were selected corresponding to the triax on the Krystall module. This was an obvious choice due to the

location's proximity to the actual Mir/Shuttle docking point. Therefore, it assumed that the number of sensors is equal to the number of inputs, meaning that the inverse system eigenvalues approximate the forward system transmission zeros. The number of desired sensor locations, n_d, is then 16 in the following analyses.

A. Application to Combined Docking Events

In an effort to predict the RSS pulse response based solely on docking data, all three docking data sets were combined such that $n_s = n_a = n_e = 3$. This obviously assumes that the Mir structure is identical for all three docking events and the computed result would not directly lend itself to the identification of any damage that may have occurred between STS-81 and STS-89. The RSS pulse response was computed using Eq. (11) in which the data matrix Y_s possessed 650 block rows and 1,100 block columns. Normally distributed zero mean random noise, equivalent to 1.0% of the rms response, was added to Y_s to stabilize the computation of the pseudo inverse. The same computation was performed using the FEM simulated docking data discussed in Section III. Both sets of pulse responses were low-pass filtered to 5.0 Hz. Figure 6 compares the FEM and Mir data based pulse responses at 104014z (Kvant-2) due to input at 105011z (Krystall). The agreement is quite good over the first several seconds, after which the response based upon real data damps out more quickly. This result is consistent with the higher than expected levels of damping found by Kim and Kapok in the analysis of data produced by the Mir Structural Dynamics Experiment (MiSDE) [2] and Shultz in the analysis of docking loads [20]. Figure 7 presents another comparison of FEM and Mir pulse responses at 102015z (Kvant) due to input at 105011z. The agreement is certainly good qualitatively, with quantitative agreement on the high frequency component of the vibration. Overall, FEM/Mir correlation was best for responses in the *z* direction due to input in the *z* direction at 105011. This is consistent with the fact that the *z* direction corresponds to the docking axis and thus the maximum input force.

Mir inverse system modal parameters were estimated by applying ERA to the computed RSS pulse response after low-pass filtering. Results are listed in Table 5. Four normal modes were extracted from the combined docking data pulse responses with modal amplitude coherence and modal phase collinearity greater than 0.74 and 80.0, respectively. Various combinations of numbers of block rows and block columns in the Hankel matrix, and numbers of retained singular values were used in the ERA analysis. Modes 1 and 3 were computed using 40 block rows and 500 block columns with 180 singular values, while modes 2 and 4 were computed with 50 block rows, 600 block columns, and 80 retained singular values. The mode singular value indicates that modes 1 and 2 were the most strongly excited modes in their respective analyses. Table 6 lists the self-MAC for the four identified mode shapes. Off-diagonal terms indicate that the shapes are relatively independent with the largest coupling occurring between modes 1 and 4.

As discussed previously, for the present case, the inverse system eigenvalues and mode shapes correspond to the forward system transmission zeros and their corresponding forced shapes in which the *xyz* translations at the reference location 105011 are fixed. In general, the transmission zero shapes do not correspond to normal modes of the forward system structure.

However, due to the dominance of the measured response by the input along the *z* axis and the high relative stiffness of the structure along this direction, information transmission is very fast between the docking point 118009 and the reference sensor location on Krystall. It is therefore believed that the system should behave in many respects as though the input and reference sensor locations are collocated. At least some of the transmission zero shapes dominated by the *z* direction should correspond to normal modes of Mir with 105011xyz fixed.

Test-analysis correlation was performed between the four identified test modes and 208 FEM modes computed with the translations at 105011 constrained. Based upon frequency and cross-MAC, the first two test modes were matched with FEM modes 80 and 91, respectively. As in the numerical simulation, a Modal TAM was generated for FEM modes 80 and 91 and then cross-orthogonality was computed between the test and corresponding FEM mode shapes. Correlation results are listed in Table 7. Based upon frequency errors of approximately 3.0% and less, MAC values greater than 80.0, and cross-generalized mass values greater than 90.0, it is believed that the FEM accurately predicts the first two modes identified from the combined docking data set. Note that FEM modes 80 and 91 computed with translations at reference node 105011 fixed are essentially the same in shape and frequency as FEM modes 80 and 91 computed earlier in the numerical simulation with the docking node 118009 translations fixed. Therefore, the identification results produced by the combined docking data sets is very analogous to the results produced in the simulation in which modes 80 and 91 are predominant and accurately identified. Noting that over 80.0% of the strain energy in FEM mode 80, and to a much lesser degree in mode 91, is concentrated in the Spektr- and Kvant-2-to-base module interfaces, accurate test-analysis correlation of these two modes tends to indicate that at least these interfaces in Mir are undamaged with respect to bending stiffness.

B. Application to Individual Docking Events

A drawback of the approach presented for identifying the RSS pulse response and subsequent modal identification is the requirement that the number of experiments coincides with the number of force inputs. This requirement is particularly troublesome in the case of post-damage modal identification for subsequent damage detection. For the example considered, it would be very desirable to be able to detect damage after one additional post-damage docking event rather than waiting for additional docking data sets such that the complete post-damage RSS pulse response can be detected.

In the previous section, all three docking data sets were combined to produce an estimate of the RSS pulse response. More block columns than block rows had to be used in the combined data matrix to stabilize the computation in Eq. (11). Therefore, the projected pulse response $\hat{P}_i$ computed in Eq. (12) using only the *i*th data set does not coincide with the projection of the pulse response P onto the column space of the *i*th data set. A direct comparison of P_i and $\hat{P}_i$ cannot be used to detect damage from one individual data set to the next. However, individual docking data sets can be used for damage detection in an a posteriori fashion. It is assumed that P_{FEM}, produced by FEM docking simulations, represents the undamaged structure, and P_{Mir}, produced in Section

IV.A by combining the real docking data, represents the structure identified by the latest three docking events. Individual docking data sets STS-81, STS-89, and STS-91 can be used to detect inter-docking event structural damage by comparing the orthogonal projections of each of the pulse responses onto the corresponding data set. If the projections satisfy

$$P_{FEM}H_i \approx P_{Mir}H_i \tag{17}$$

for the *i*th data set, then the response produced by the corresponding docking event still reflects the undamaged structure. If the projected pulse response correlation is poor, this is evidence that a structural change has occurred. If agreement is good for all three docking data sets, there is strong evidence that structural damage has not occurred. Of course, another possibility is that damage is present, but the act of docking doesn't excite it.

Equation (17) was applied for all three docking data sets. The orthogonal projectors H_i were computed using Eq. (13) and a data matrix Y_{si} with 650 block rows and columns. Figure 8 illustrates the Mir and FEM pulse responses from 105001z to 104014z projected onto data from STS-81 after low pass filtering to 5.0 Hz. The agreement is quite good, indicating that the response produced by STS-81 still reflects an undamaged Mir structure. This is consistent with the results produced by Kim and Kapok [2] and the fact that STS-81 preceded the Progress collision. This is also consistent with the good test-analysis correlation presented in Section IV.A for FEM mode 80 which dominates the response at 104014z. Figure 9 presents the Mir and FEM pulse responses from 105001z to 104014z projected onto data from STS-89, which took place after the collision. Once again, the agreement is very good, indicating that response from STS-89 accurately reflects the undamaged Mir structure at least with respect to the *x* axis torsional springs at the Spektr and Kvant-2 interfaces to the core module that dominate the strain energy in FEM mode 80. Mir and FEM pulse responses from 105001z to 101022z (Base Block) projected onto data from STS-89 are illustrated in Fig. 10. The correlation between projected FEM and Mir pulses responses at this location is also quite good, again indicating that response from STS-89 reflects the undamaged structure. Comparable agreement between projected Mir and FEM pulse responses was also found for the other *z* sensor locations for STS-89.

Finally, the pulse responses were projected onto data from STS-91. Figure 11 shows the projection of the pulse responses from 105001z to 104014z. Agreement is still very good for the response at 104014z. Figure 12 compares the projected responses at 101022z. The correlation is not as good for this response, but qualitatively the projections are very comparable. It is believed that the data from STS-91 also reflects the response of an undamaged Mir structure to docking loads. Weighing all the results produced by comparing the Mir and FEM pulse responses, their projections on individual data sets, and modal identification results, it appears that Mir was in an undamaged state, at least with respect to docking excitation, at the time of STS-91. This observation is in agreement with the overall results and observations produced by Kim and Kapok in the Boeing MiSDE analysis [2]. The significance of the contribution of the RSS approach is that it arrived at the same conclusion using not only a different set of sensor locations, but also a totally

different type of excitation. The MiSDE work did not consider Mir/Shuttle docking because capture of the Shuttle is not instantaneous, resulting in a nonstationary system with nonlinear dynamic behavior. The RSS method is not affected by these problems and therefore compliments the MiSDE work.

V. Conclusion

The goal of this work was to determine if it is feasible to use Mir/Shuttle docking data to perform Mir damage detection. A time-domain technique called Remote Sensing was proposed as an approach. The method uses inverse structural dynamics to identify physical characteristics which can subsequently be used for damage detection. The term "inverse" refers to the fact that the roles of input and output are reversed from the usual forward system structural dynamics problem. If sensors such as accelerometers are placed at the external input locations, modal parameters corresponding to structural motion with the sensor locations fixed can be identified. If sensors are not collocated with the inputs, other important structural characteristics can be determined such as transmission zeros and their corresponding shapes. The RSS method was demonstrated for a numerical simulation of Mir/Shuttle docking assuming that sensors were collocated with the Mir docking location. Several fixed interface Mir modes were identified from the computed RSS pulse responses using ERA, and then correlated with the FEM. The method was then applied to the combined set of docking data from STS-81, STS-89, and STS-91. Even though there were no sensors available at the docking point, ERA produced two modes that correlated very well with FEM fixed interface modes that were also accurately identified in the numerical simulations. Finally, projections of the Mir and FEM RSS pulse responses onto the individual docking data sets were compared for changes in the structure. Overall, the results produced by this work appear to indicate that Mir was in an undamaged state, at least with respect to docking excitation, at the time of STS-91. There is an especially high level of confidence in the undamaged state of the Spektr- and Kvant-2-to-base module interfaces. This observation is in agreement with the overall results and observations produced in the Boeing MiSDE analyses.

The significance of the contribution of the RSS approach is that it was able to produce the same conclusion using not only a different set of sensor locations, but also a totally different type of excitation. Mir/Shuttle docking event data was not considered in the MiSDE work because capture of the Shuttle is not instantaneous, resulting in a nonstationary system with nonlinear dynamic behavior. The RSS method is not affected by these problems and therefore provides a strong compliment to the methods and procedures used in the MiSDE work. Another important advantage of this approach is that it only requires measured response data. The applied external forces or internal interface forces are not required for modal identification. This characteristic makes the Remote Sensing System approach applicable in cases where the input forces cannot be measured. It is believed that RSS provides a valuable new method to identifying characteristics of structures from measured data without the need for measuring the input.

Acknowledgments

This work was supported by NASA Johnson Space Center under Grant NAG9-953. The authors would like to thank contract monitor Mr. James Dagen for his support and encouragement. They would also like to express appreciation to Rocket and Space Corporation-Energia (RSC-E) for providing the Mir FEM and flight data, and Mr. Ken Shultz of Lockheed Martin Corporation.

References

[1] Doebling, S. W., C. R. Farrar, M. B. Prime and D. W. Shevitz, "Damage Detection and Health Monitoring of Structural and Mechanical Systems from Changes in Their Vibration Chracteristics: A Literature Review," Los Alamos National Laboratory, LA-13070-MS, 1996.

[2] Kim, H. and M. Kaouk, "Mir Structural Dynamics Experiment," The Boeing Company, Contract No. NAS15-10000, 1998.

[3] Juang, J. and R. S. Pappa, "An Eigensystem Realization Algorithm for Modal Identification and Model Reduction," *Journal of Guidance, Control, and Dynamics*, **8**(5), 1985, pp. 620-627.

[4] James, G. H., T. G. Carne and J. P. Lauffer, "The Natural Excitation Technique (NExT) for Modal Parameter Extraction form Operating Structures," *Modal Analysis*, **10**(4), 1995, pp. 260-277.

[5] Overschee, V. and B. DE Moor, "N4SID: Subspace Algorithms for the Identification of Combined Deterministic-Stochastic Systems," *Autimatica*, **30**(1), 1994, pp. 75-93.

[6] Kammer, D. C. and A. D. Steltzner, "Structural Identification using Inverse System Dynamics," *17th International Modal Analysis Conference*, Kissimmee, FL, SEM, 1999, pp. 1880-1886.

[7] Kammer, D. C., "Estimation of Structural Response Using Remote Sensor Locations," *Journal of Guidance, Control, and Dynamics*, **20**(3), 1997, pp. 501-508.

[8] Williams, T., "Transmission-Zero Bounds for Large Space Structures, with Applications," *Journal of Guidance, Control, and Dynamics*, **12**(1), 1989, pp. 33-38.

[9] Cannon, R. H. and D. E. Rosenthal, "Experiments in Control of Flexible Structures with Noncolocated Sensors and Actuators," *Journal of Guidance, Control, and Dynamics*, **7**(5), 1984, pp. 546-553.

[10] Craig, R. R. and M. C. C. Bampton, "Coupling of Substructures for Dynamic Analysis," **6**(7), 1968, pp. 1313-1319.

[11] Juang, J. N., *Applied System Identification*, Prentice Hall, Englewood Cliffs, NJ, 1994.

[12] Juang, J.-N., M. Phan and R. W. Longman, "Identification of Observer/Kalman Filter Markov Parameters: Theory and Experiments," *Journal of Guidance, Control, and Dynamics*, **16**(2), 1993, pp. 320-329.

[13] Horta, L. G. and C. A. Sandridge, "On-Line Identification of Forward/Inverse Systems for Adaptive Control Applications," *AIAA Guidance, Navigation, and Control Conference*, , 1992, pp. 1639-1649.

[14] Ben-Israel, A. and T. N. E. Greville, *Generalized Inverses: Theory and Applications*, John Wiley & Sons, New York, 1974.

[15] Pappa, R. S., K. B. Elliot and A. Schenk, "A Consistent-Mode Indicator for the Eigensystem Realization Algorithm," *33rd AIAA/ASME/ASCE/AHS/ASC Structures, Structural Dynamics and Materials Conference*, Dallas, TX, 1992, pp. 556-565.

[16] Ewins, D. J., *Modal Testing: Theory and Practice*, John Wiley & Sons, New York, 1984.

[17] Kammer, D. C., "Test-Analysis Model Development Using an Exact Modal Reduction," **2**(4), 1987, pp. 174-179.

[18] Kammer, D. C., and Triller, M. J., "Ranking the Dynamic Importance of Fixed Interface Modes using a Generalization of Effective Mass," *International Journal of Analytical and Experimental Modal Analysis*, **9**(2), 1994, pp. 77-98.

[19] Steltzner, A. D. and D. C. Kammer, "Input Force Estimation Using an Inverse Structural Filter," *17th International Modal Analysis Conference*, Kissimmee, FL, SEM, 1999, pp. 954-960.

[20] Shultz, K. P., "Loads Analysis for Space Shuttle Docking to Mir," *30th AIAA Structures, Structural Dynamics, and Materials Conference*, Kissimmee, FL, 1997, pp. 555-565.

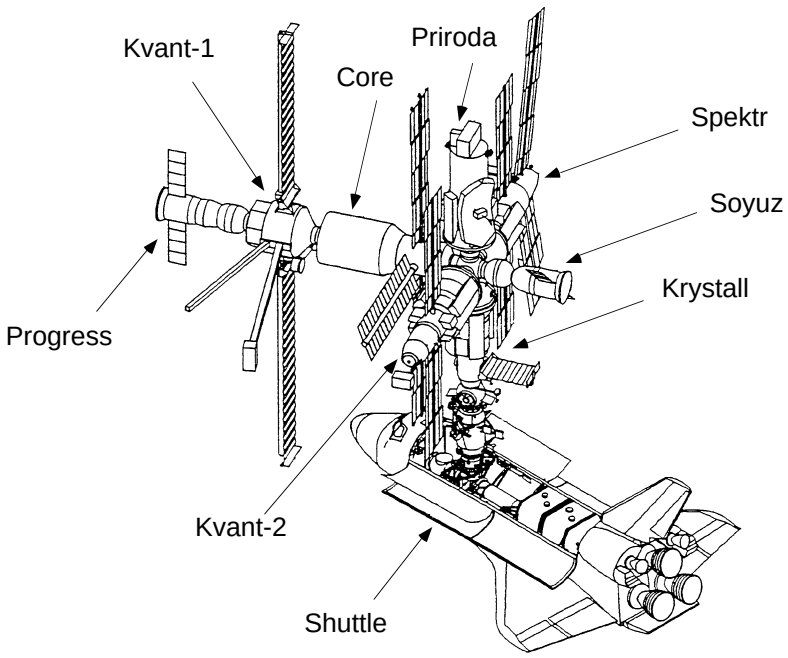

Fig. 1. Shuttle-Mir mated configuration.

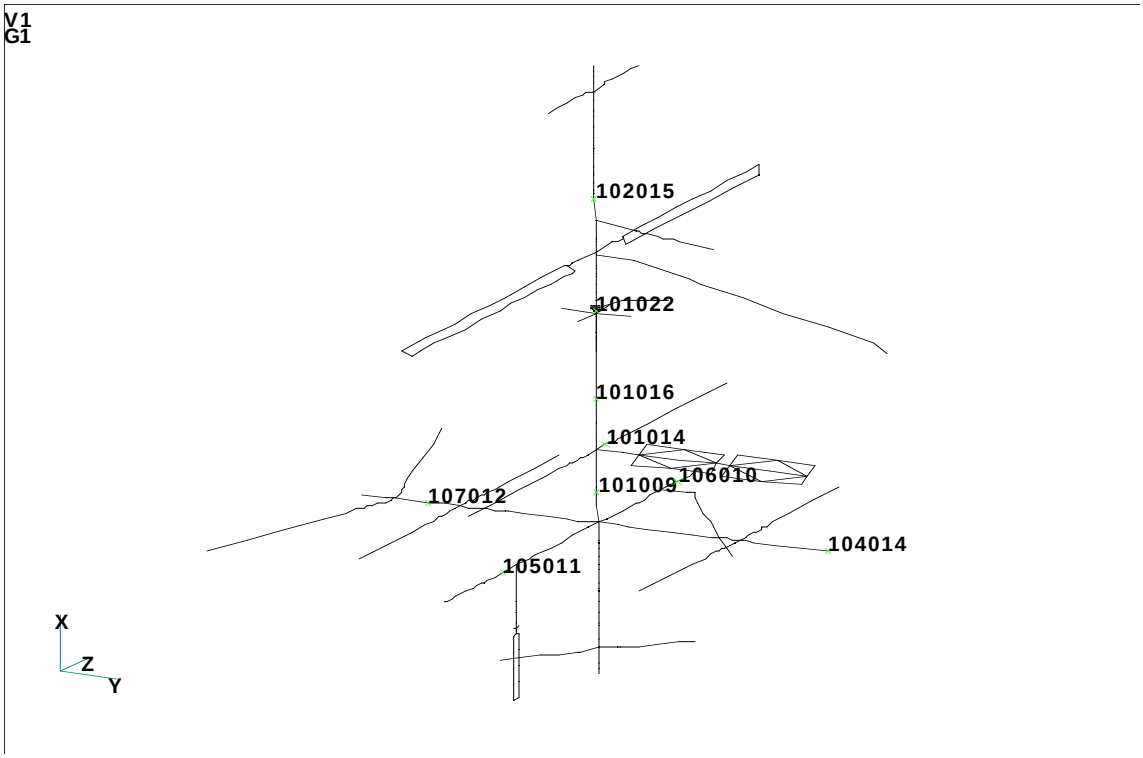

Fig. 2. Mir finite element model.

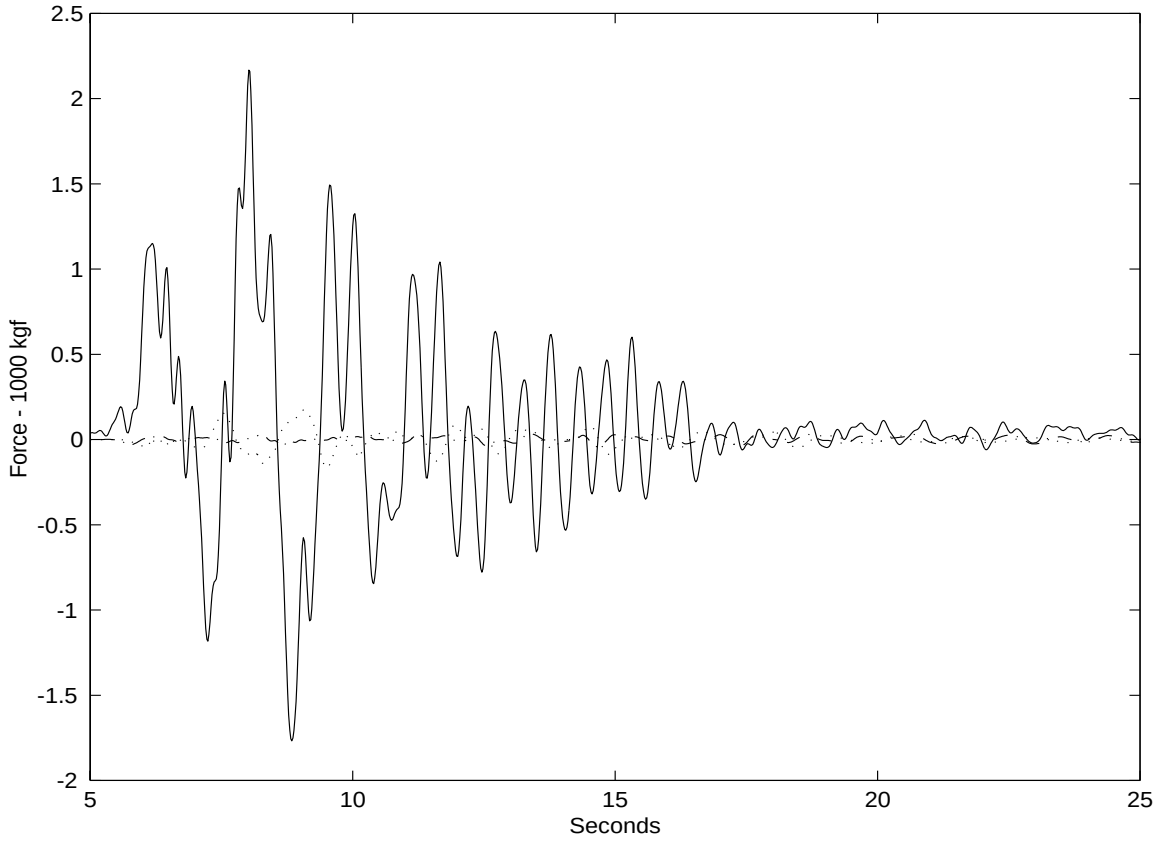

Fig. 3. Simulated docking forces for experiment 1. ..... x, -.-.- y, ____ z

Table 1. Accelerometer listing for STS-81

Channel No.	Location	Index	Direction	Node No.
1	Base Block	NP1	y	101009
2	Base Block	BP1	z	101009
3	Base Block	OP1	x	101009
4	Base Block	NP2	y	101014
5	Base Block	BP2	z	101014
6	Base Block	NP3	y	101016
7	Base Block	BP3	z	101016
8	Base Block	NP4	y	101022
9	Base Block	BP4	z	101022
10	Base Block	OP4	x	101022
11	Kvant	NPE	y	102015
12	Kvant	BPE	z	102015
13	Kvant	OPE	x	102015
14	Priroda	NPI	y	106010
15	Priroda	BPI	x	106010
16	Priroda	OPI	z	106010
17	Spektr	NPO	x	107012
18	Spektr	BPO	z	107012
19	Spektr	OPO	y	107012
20	Kvant-2	NPD	x	104014
21	Kvant-2	BPD	z	104014
22	Kvant-2	OPD	-y	104014
23	Kristall	NPT	y	105011
24	Kristall	BPT	-x	105011
25	Kristall	OPT	z	105011

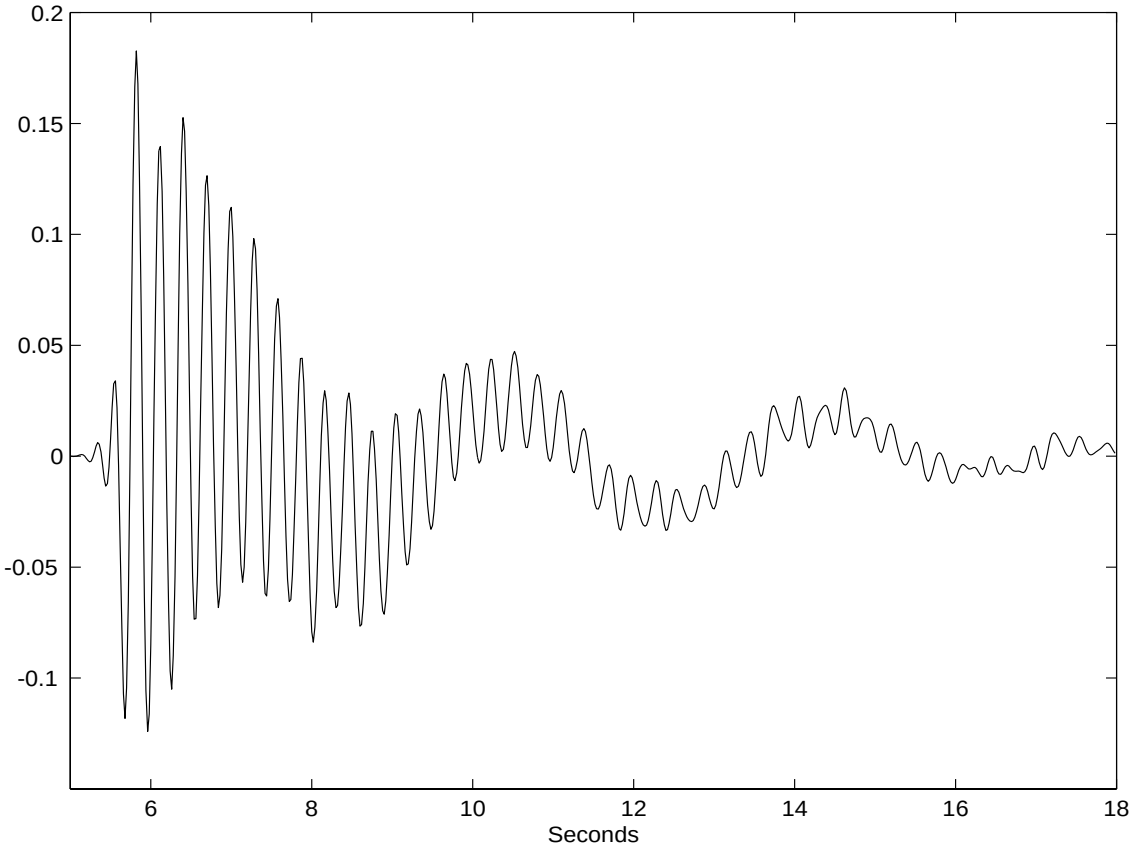

Fig. 4. Mir RSS pulse response from 118009z to 102015z.

Table 2. Modal identification results for simulated docking event.

Mode	Damping	Freq. (Hz)	MAmpC	MPC	MSV
1	2.3662e-02	9.6790e-01	9.9658e-01	9.6648e+01	1.0000e+00
2	3.7093e-02	1.2574e+00	8.2249e-01	9.5149e+01	4.6777e-01
3	4.1464e-02	2.5970e+00	8.6669e-01	9.5024e+01	3.8999e-01
4	3.3820e-02	2.6738e+00	8.9253e-01	8.8143e+01	4.4705e-01
5	2.3423e-02	3.3993e+00	9.8848e-01	9.7884e+01	5.6949e-01

Table 3. Self-MAC results for identified mode shapes.

Mode	1	2	3	4	5
1	100.00	0.58	0.01	0.62	0.06
2		100.00	2.45	0.21	0.01
3			100.00	9.83	0.03
4				100.00	0.04
5					100.00

Table 4. Correlation between estimated docking modes and fixed FEM.

Estimated Docking		FEM				Cross
Mode	Freq.	Mode	Freq.	% Error	MAC	Gen. Mass
1	0.968	80	0.953	1.57	98.51	84.30
2	1.257	91	1.216	3.37	89.86	86.57
3	2.597	143	2.498	3.96	99.36	87.09
4	2.674	144	2.578	3.72	91.51	95.55
5	3.399	170	3.395	0.12	97.43	100.00

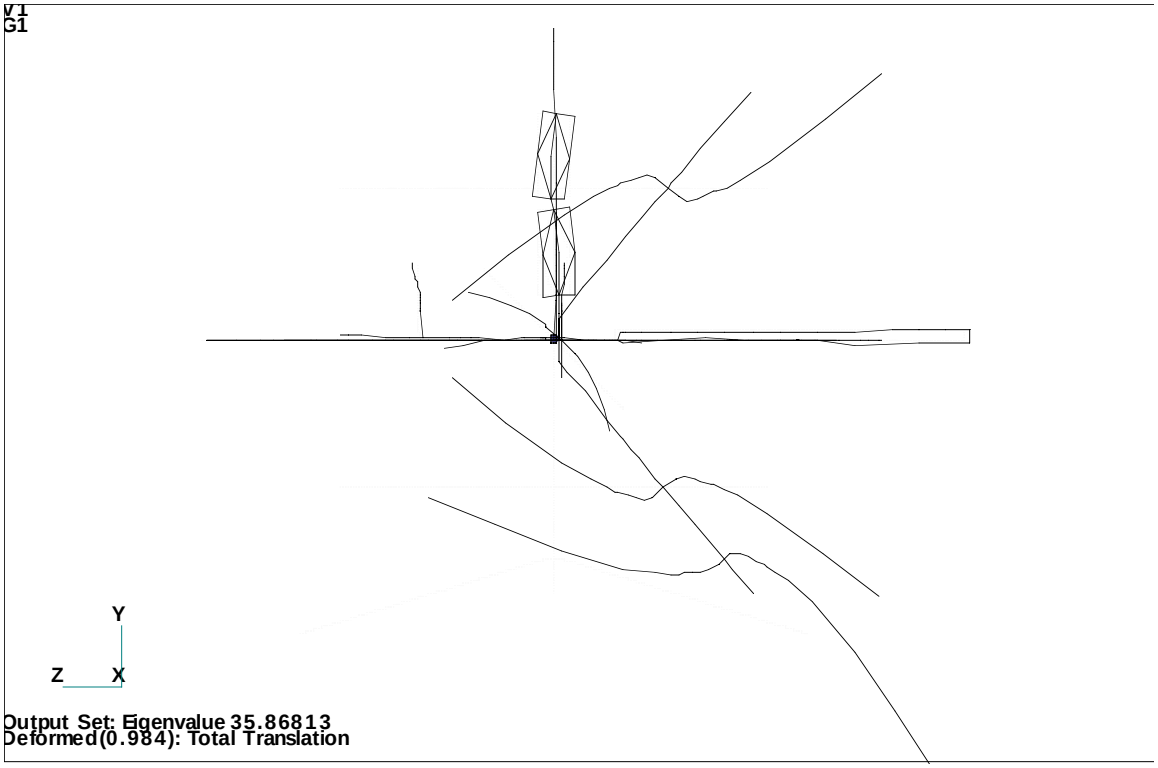

Fig. 5. Mir FEM mode 80 with translations at docking node 118009 fixed, 0.953 Hz.

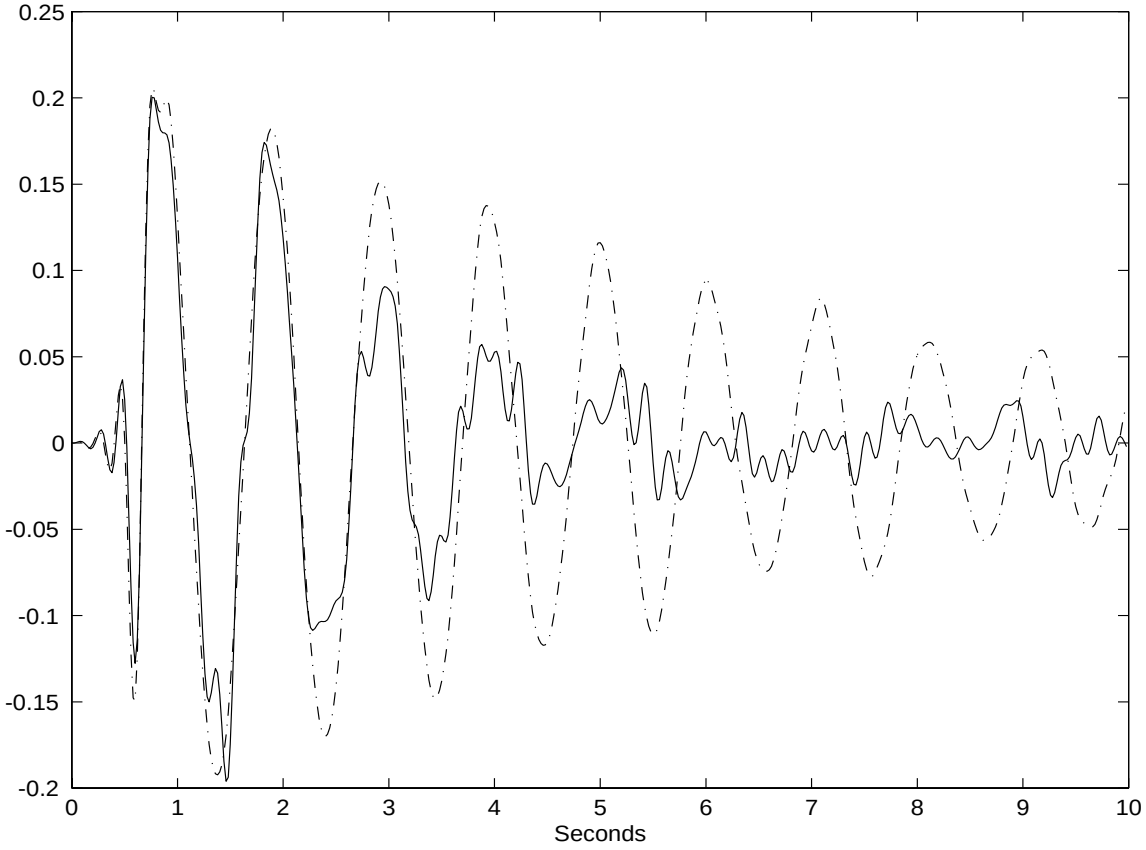

Fig. 6. RSS pulse response, 105011z (Krystall) to 104014z (Kvant-2). ____ Mir, -.-.-. FEM

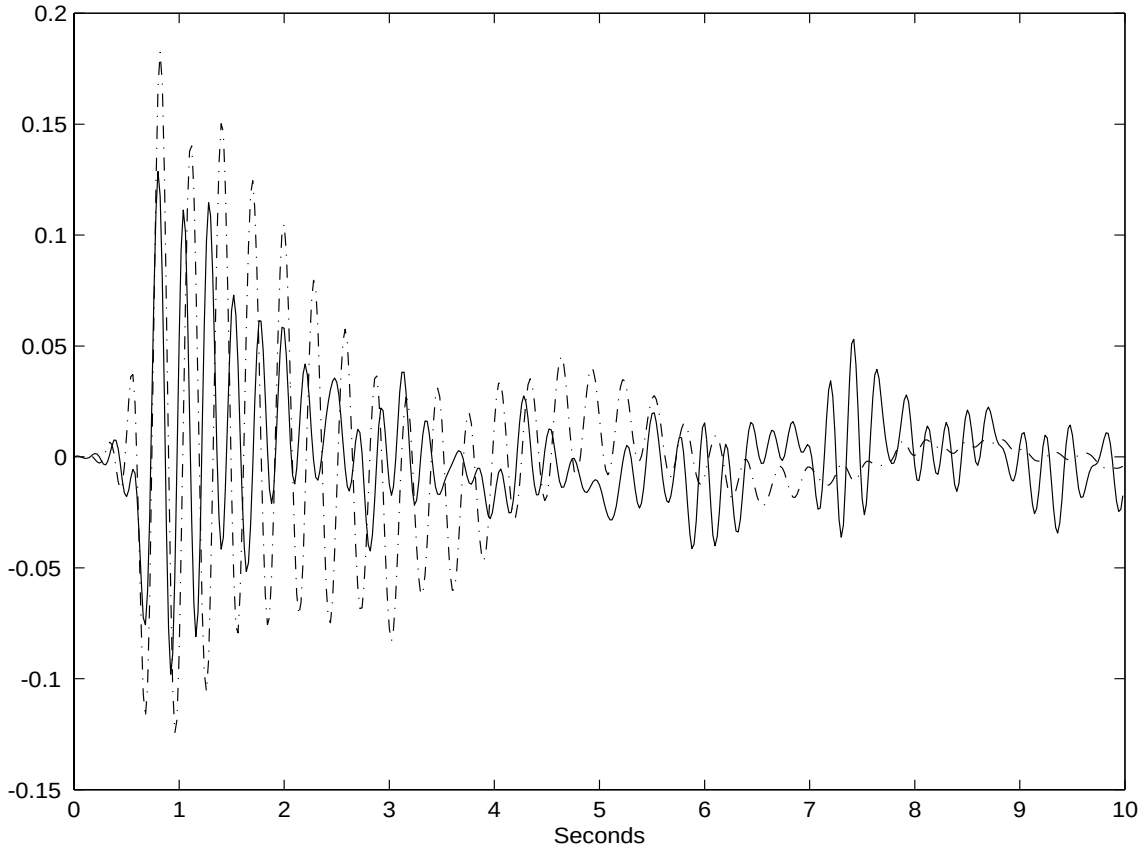

Fig. 7. RSS pulse response, 105011z (Krystall) to 102015z (Kvant). ____ Mir, -.-.-. FEM

Table 5. Modal identification results using combined docking data.

Mode	Damping	Freq. (Hz)	MAmpC	MPC	MSV
1	7.600e-02	9.946e-01	9.725e-01	9.034e+01	1.000e+00
2	3.462e-02	1.203e+00	8.240e-01	8.508e+01	1.000e+00
3	3.120e-02	1.364e+00	9.245e-01	8.771e+01	5.409e-01
4	2.483e-02	4.581e+00	7.400e-01	8.034e+01	4.635e-01

Table 6. Self-MAC results for identified mode shapes.

Mode	1	2	3	4
1	100.00	7.25	1.22	24.43
2		100.00	16.42	2.48
3			100.00	0.36
4				100.00

Table 7. Correlation between estimated docking modes and fixed FEM.

Estimated Docking		FEM				Cross
Mode	Freq.	Mode	Freq.	% Error	MAC	Gen. Mass
1	0.995	80	0.962	3.32	98.61	90.80
2	1.203	91	1.219	-1.33	81.54	99.60

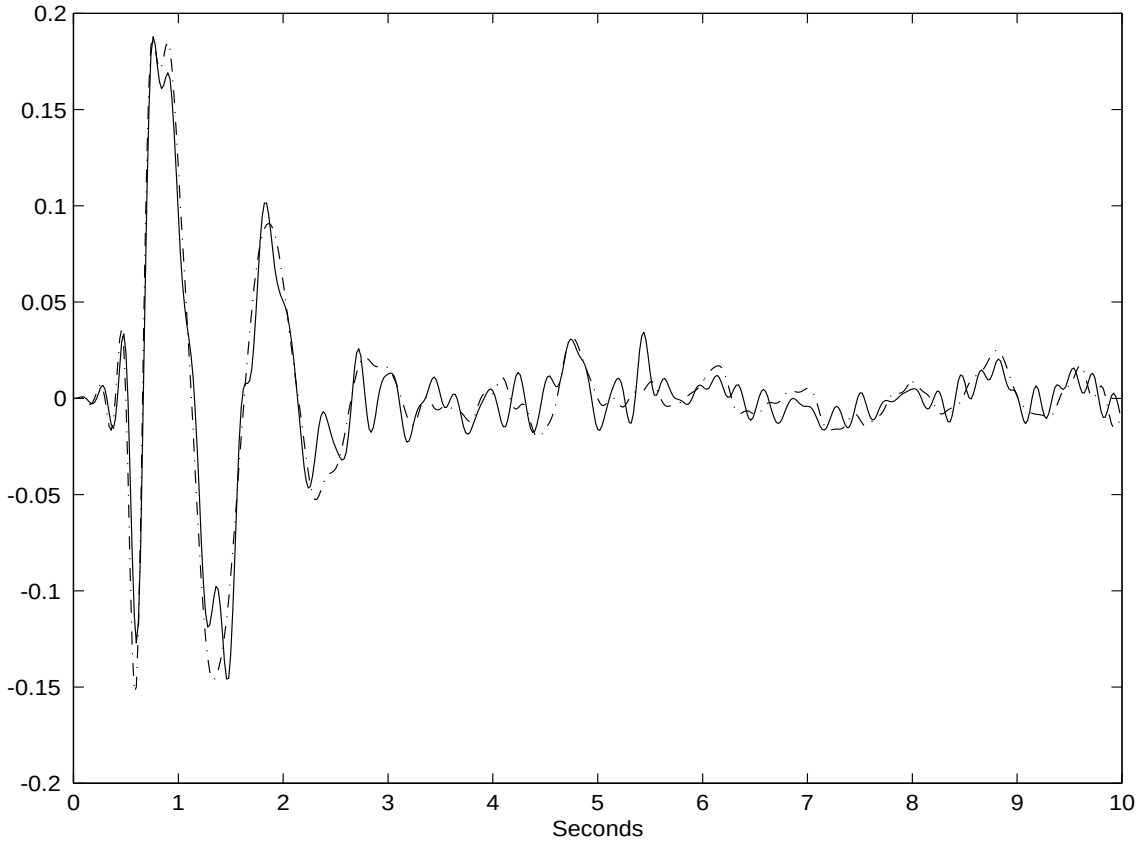

Fig. 8. Pulse responses at 104014z projected onto STS-81 data set. ____ Mir, -.-.-. FEM

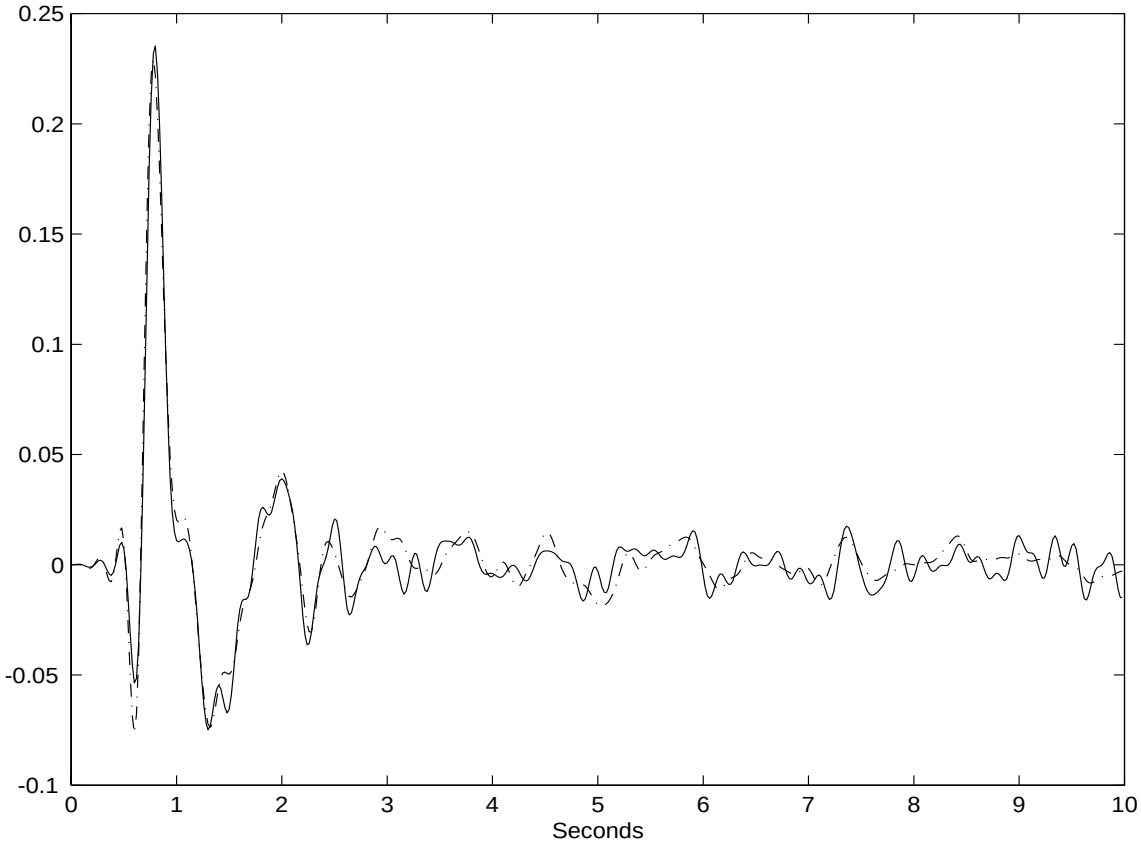

Fig. 9. Pulse responses at 104014z projected onto STS-89 data set. ____ Mir, -.-.-. FEM

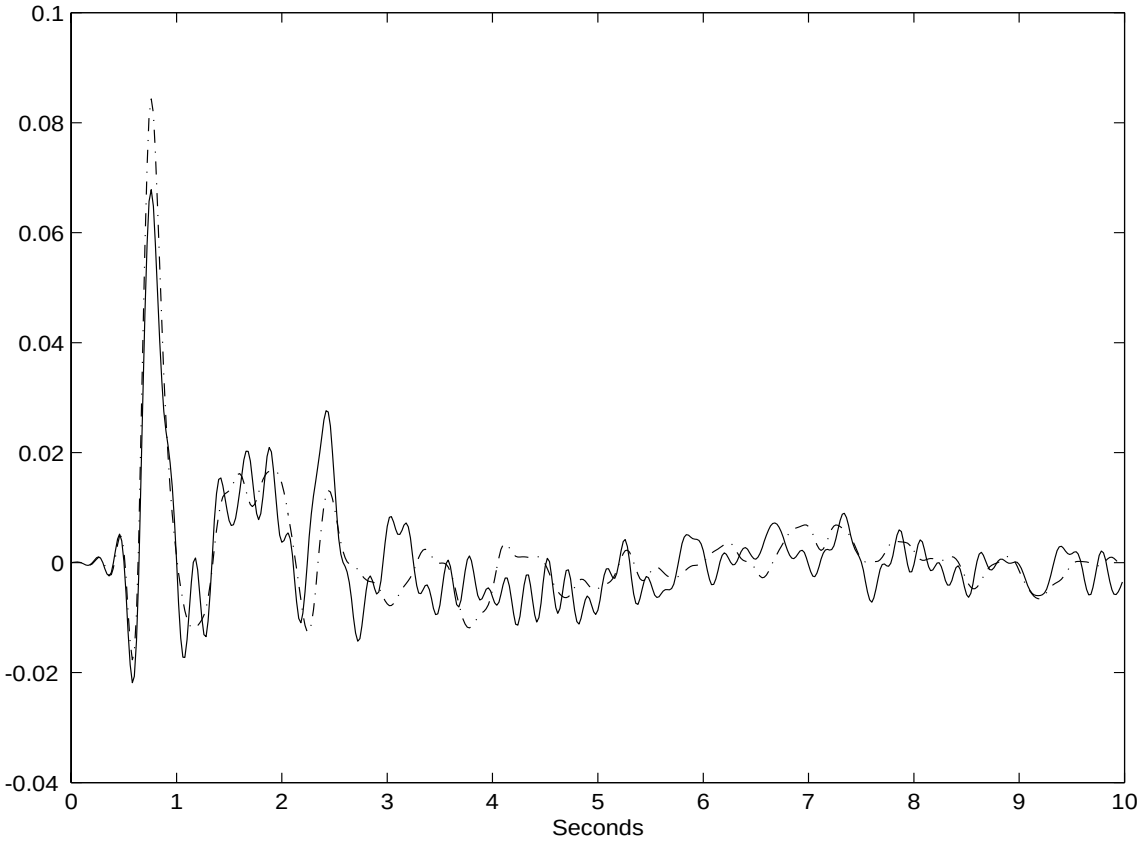

Fig. 10. Pulse responses at 101022z (Base Block) projected onto STS-89. ___ Mir, -.-.-. FEM

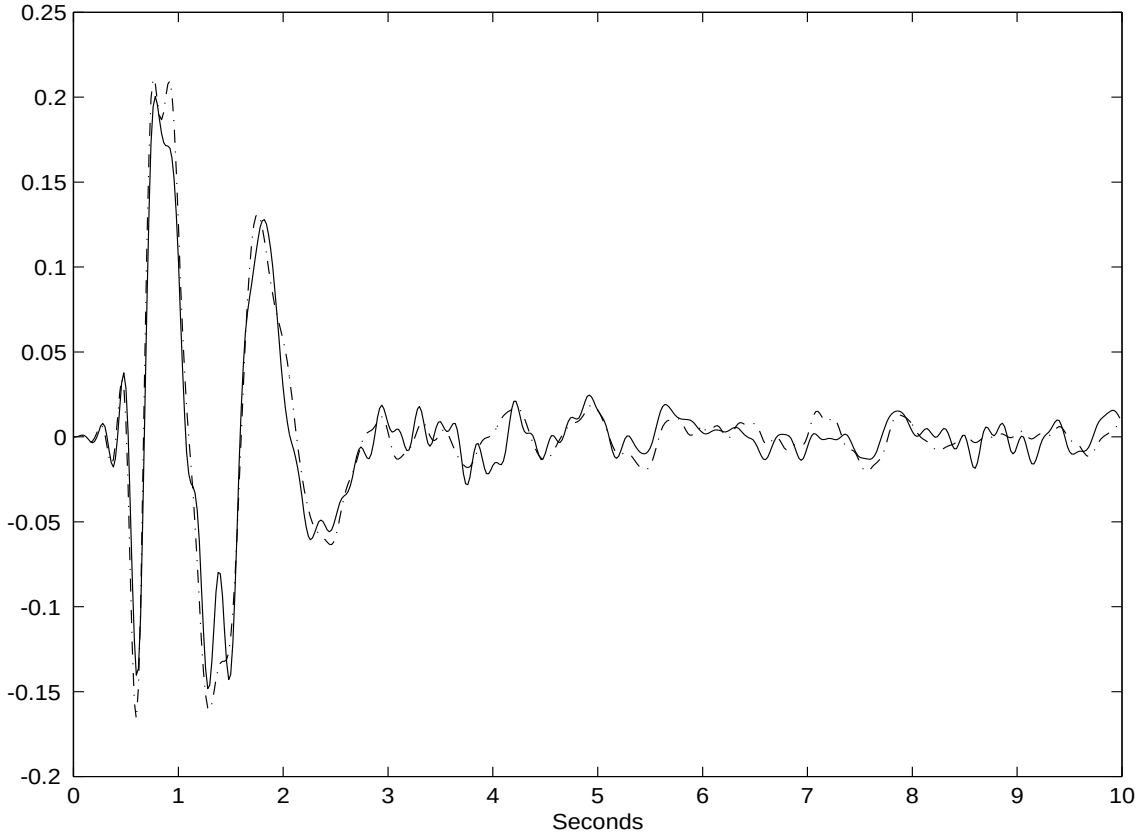

Fig. 11. Pulse responses at 104014z projected onto STS-91. ___ Mir, -.-.-. FEM

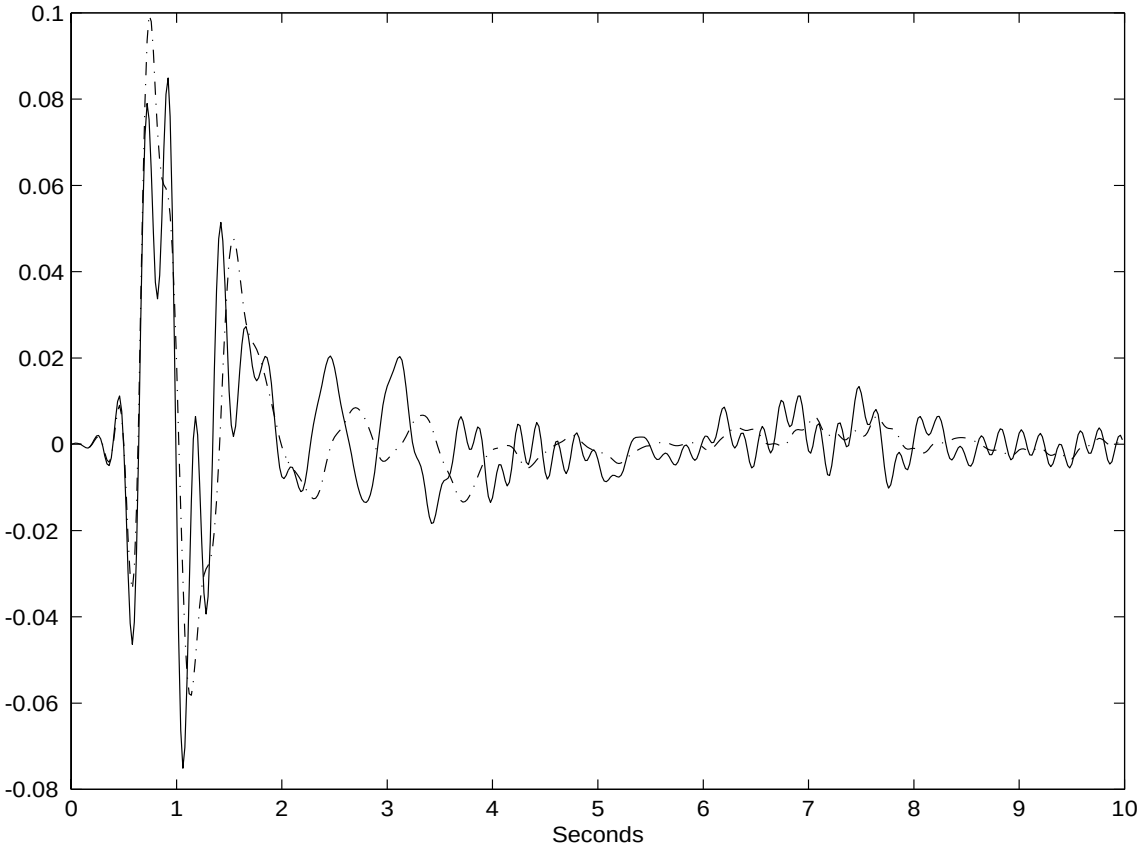

Fig. 12. Pulse responses at 101022z (Base Block) projected onto STS-91. ___ Mir, -.-.-. FEM